COBEM 2021 26th International Congress of Mechanical Engineering
ABCM Associação Brasileira de Engenharia e Ciências Mecânicas
November 22-26, 2021, Virtual Congress, Brazil

COB-2021-0059
Comparison between two singularity Avoidance Indices for Planar Parallel Kinematically Redundant Manipulators

Felipe Marques Farias Filho
Maíra Martins da Silva
University of São Paulo, São Carlos School of Engineering, Av. Trabalhador São-carlense, 400, CEP 13566-590 - São Carlos, SP - Brasil
fmfariasfilho@usp.br, mairams@sc.usp.br

João Vitor de Carvalho Fontes
Federal University of São Carlos, Rodovia Washington Luís, km 235 - SP-310, CEP 13565-905 - São Carlos, SP - Brasil
joaofontes@ufscar.br

Abstract. *Parallel manipulators (PMs) have potential advantages compared to their serial counterparts, such as higher accuracy, higher stiffness, higher dynamic performance, and high load capacity to mass ratio. The main drawback is their limited workspace and the presence of singularities within it. Kinematic redundancy might reduce the presence of singular regions, but the inverse kinematic problem of kinematically redundant PMs present infinite solutions. Therefore, an optimization problem, denoted as redundancy resolution, can be stated, aiming to select the best solution among the others. Adequate performance indices, among them singularity avoidance indices, should compose the objective function. One of the most commonly used is the inverse of the condition number of the end-effector's Jacobian matrix, also known as the Local Conditioning Index (LCI). Another candidate is the Normalised Scaled Incircle Radius (NSIR), based on the manipulator's geometrical characteristics and the inverse kinematics Jacobian matrix. This work aims to compare the use of indices in redundancy resolution schemes of a planar parallel kinematically redundant manipulator, the 3PRRR. The prepositioning and the ongoing redundancy resolution schemes and four pre-defined end-effector trajectories, straight line, circle, spiral, and square, are numerically investigated. The optimization algorithm used for redundancy resolution is solved offline by exploring Genetic Algorithms (GA) and Sequential Quadratic Programming (SQP). The design variables are the positions of the redundant active joints. Whilst NSIR obtains better performance indices, it takes longer to be derived since it requires more calculations. Therefore, the LCI should be preferred for real-time applications, while the NSIR would be more advantageous for offline applications.*
Keywords: *Redundancy Resolution, Normalised Scaled Incircle Radius, Local Conditioning Index, Optimization, Robotics.*

1. INTRODUCTION

When compared to serial manipulators, parallel manipulators have certain advantages, such as agility, high rigidity, high accuracy, high payload-to-weight ratio (Ebrahimi *et al.*, 2008b). But they do have drawbacks, such as small workspaces, complex kinematics, and numerous singularities within their workspace. The latter can be defined as configurations in which the end-effector has uncontrolled Degrees-Of-Freedom (DOF) (Merlet, 2006). These singularities reduce the useful workspace of the manipulator, resulting in a low ratio between the useful workspace and the installation space.

To minimize or overcome this problem, the use of redundant manipulators have been investigated. According to Gosselin and Schreiber (2018), there are two main types of redundancies that can be added to parallel manipulators. The first type is the actuation redundancy characterized by introducing kinematic chains to the mechanism or adding actuators to passive joints. This kind of redundancy might lead to high internal forces. The second type is the kinematic redundancy implemented by adding at least one active joint to a kinematic chain. Figure 1 illustrates both redundancy types. The 3RRR is a non-redundant planar PM, 4RRR is a planar PM with actuation redundancy and the 2RRR+PRRR is a planar kinematically redundant, where R and P stand for revolute and prismatic joints, respectively, and the underlined letters indicate the active joints.

Kinematic redundancies add DOFs to the manipulator and produce an infinite number of solutions to the inverse displacement problem (Ebrahimi *et al.*, 2008b), as illustrated in Fig. 1(d). This gain in mobility is helpful not only for singularity avoidance but also for workspace enlargement. However, a scheme for determining the best solution among all others should be exploited. This strategy is called redundancy resolution and can be formulated as an optimization problem. In the objective function of such problems, manipulators' local performance measures are used, *i.e.*, indices that

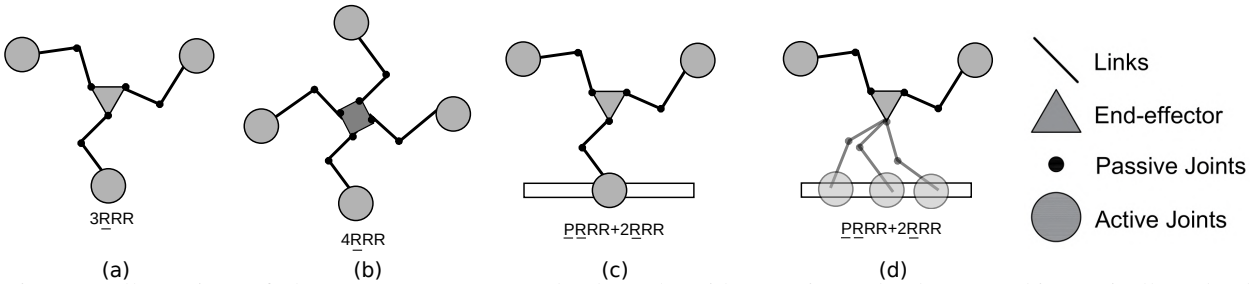

Figure 1: Illustrations of planar PMs: (a) a non-redundant, (b) with actuation redundancy, (c) kinematically redundant, and (d) reconfiguration capability of the redundant kinematically PM

depend on the posture of the manipulator (Patel and Sobh, 2014).

Singularity avoidance indices are among the performance measurements that should compose the objective function of redundancy resolution schemes. Several singularity avoidance indices have been reported in the literature like the Condition Number, Manipulability index, Minimum Singular Value (MSV) and others (Patel and Sobh, 2014). One of the most commonly used is the Local Conditioning Index (LCI), as mentioned in Alba-Gomez *et al.* (2005); Wu *et al.* (2011); Xie *et al.* (2014); Patel and Sobh (2014). It has the advantage to be available for all manipulators, it is bounded between zero and the unity, and it is easily calculated. But it is also pointed out that it has many drawbacks, such as coordinate system (frame) dependency, absence of explicit geometric meaning, and that for manipulators with more than one type of actuation, it is necessary to homogenize the Jacobian matrix.

Several articles have introduced new indices, Wu *et al.* (2011), for example, presented several indices which take into account motion/force transmission. Yao *et al.* (2018) proposed a new global index for mechanical design optimization. And Xie *et al.* (2014), which presented a new performance measure based on the reciprocal product of screw theory. Among these, Ebrahimi *et al.* (2008b) defined a new local singularity avoidance index called Normalised Scaled Incircle Radius (NSIR). Unlike the others, it has a geometric meaning. Also, it is bounded between one and zero, and it is not dependent on the base coordinate system used. But it is only applicable to a class of planar parallel manipulators, and it is not as easily calculated as the LCI. However, in Ebrahimi *et al.* (2008b), the NSIR was compared against the condition number, which is not ideal because it is not bounded. In addition, it didn't evaluate the computation burden of each index. Therefore, the present work aims to compare both indices, LCI and NSIR, regarding redundancy resolution, considering both their computation burden and their values along their respective optimized trajectories and beginning with the kinematic analysis of the manipulator used in the comparison, a 3PRRR manipulator. This manipulator presents three levels of kinematic redundancy since three active prismatic joints have been added to the kinematic chains.

In the next section, using the results of the kinematic analysis, the Jacobian matrix is defined. Then is presented a brief explanation of the parallel manipulator's singularities based on the Jacobian matrix. After it, the LCI and NSIR indices are detailed. Then the employed redundancy resolution scheme is comprehensively elucidated. Later the results of the comparison are discussed. And finally, in conclusion, the important points of this paper are summarized.

2. INVERSE KINEMATICS AND JACOBIAN MATRIX

The following kinematic analysis of the mechanism will be explained according to Fontes and Da Silva (2016). We are initially focusing on only one of the three kinematic chains of the manipulator, as shown in Fig. 2. In the adopted notation, the subscript i refers to one of the three kinematic chains, therefore $i = 1 \dots 3$. And the subscript j represents the bodies which compose each of the kinematic chains, except for the end-effector, for which the subscript n is used. Specifically, $j = 1$ indicates the prismatic actuators in A_i, while $j = 2$ and $j = 3$ indicate respectively the links 1 and 2, also called as l_1 and l_2.

The parameters of the 3PRRR used in the simulation are shown in Tab. 1.

The base coordinate system $O - x_o y_o$ is located at the center of the manipulator's workspace and the point D is the center of the end-effector. The inverse kinematic model can obtained through the evaluation of the geometric constraint equation $\left\|\overrightarrow{B_i C_i}\right\| = \|\boldsymbol{r}_{C_i} - \boldsymbol{r}_{B_i}\| = l_2$, where $\boldsymbol{r}_{C_i}$ and $\boldsymbol{r}_{B_i}$ are the position vector of the passive joints at B_i and C_i, respectively. This restriction can be written as:

$$\left\| \begin{bmatrix} \mu_i - l_1 \cos(\theta_i) \\ \rho_i - l_1 \sin(\theta_i) \end{bmatrix} \right\| = \left\| l_2 \begin{bmatrix} \cos(\beta_i) \\ \sin(\beta_i) \end{bmatrix} \right\| = l_2 \tag{1}$$

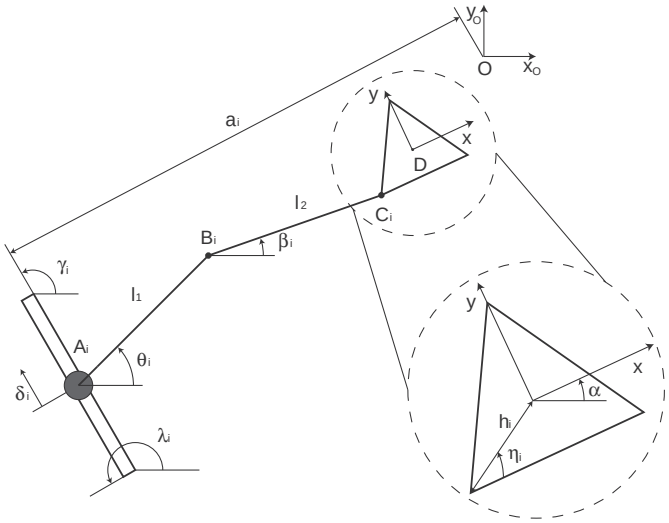

Figure 2: Representation of one of the 3PRRR's kinematic chains (Fontes and Da Silva, 2016).

Table 1: Parameters of the 3PRRR manipulator used to compare the indices.

Parameters	**Value**
a, mm	260
h, mm	59.7
η, rad	$\pi/6$
l_1, mm	191
l_2, mm	232
λ_1, rad	$\pi/2$
λ_2, rad	$11\pi/6$
λ_3, rad	$7\pi/6$
γ_1, rad	π
γ_2, rad	$\pi/3$
γ_3, rad	$5\pi/3$
Prismatic joints' upper limit (δ_{min}), mm	-230
Prismatic joints' lower limit (δ_{max}), mm	230
Prismatic joints' pitch (p), mm/turn	10

where μ_i and ρ_i are defined as:

$$\begin{bmatrix}\mu_i \\ \rho_i\end{bmatrix} = \begin{bmatrix}x \\ y\end{bmatrix} - h_i \begin{bmatrix}\cos(\alpha+\eta_i) \\ \sin(\alpha+\eta_i)\end{bmatrix} - a_i \begin{bmatrix}\cos(\lambda_i) \\ \sin(\lambda_i)\end{bmatrix} - \delta_i \begin{bmatrix}\cos(\gamma_i) \\ \sin(\gamma_i)\end{bmatrix} \tag{2}$$

where x and y represent the position of D according to the base coordinate system $O - x_o y_o$.

Equation 1 can be written as:

$$e_{i1}\sin(\theta_i) + e_{i2}\cos(\theta_i) + e_{i3} = 0 \tag{3}$$

where $e_{i1} = -2l_{1i}\rho_i$, $e_{i2} = -2l_{1i}\mu_i$ and $e_{i3} = \mu_i^2 + \rho_i^2 + (l_{1i})^2 - (l_{1i})^2$. Therefore, the angles θ_i can be obtained isolating them in Eq. 3:

$$\theta_i = 2arctan\left(\frac{-e_{i1} \pm \sqrt{e_{i1}^2 + e_{i2}^2 - e_{i3}^2}}{e_{i3} - e_{i2}}\right) \tag{4}$$

Once evaluated the angles θ_i, angles β_i can be obtained isolating them in Eq. 1, which result in the following relation:

$$\beta_i = arctan\left(\frac{\rho_i - l_1\cos(\theta_i)}{\mu_i - l_1\sin(\theta_i)}\right) \tag{5}$$

The Jacobian matrix is defined as the matrix which relates the velocity vectors of the actuators and the velocity vector of the end-effector. The velocity of the end-effector can be obtained through the time differentiation of Eq. 1:

$$\dot{x}\left[l_2\cos\left(\beta_i\right)\right]+\dot{y}\left[l_2\sin\left(\beta_i\right)\right]-\dot{\alpha}\left[l_2h_i\sin\left(\beta_i-\eta_i-\alpha\right)\right]=\dot{\theta}_i\left[l_1l_2\sin\left(\beta_i-\theta_i\right)\right]+\dot{\delta}_i\left[l_2\cos\left(\beta_i-\gamma_i\right)\right] \tag{6}$$

Equation 6 can be rewritten in matrix form as:

$$\boldsymbol{A\dot{X}=B\dot{\Theta}} \tag{7}$$

where, $\boldsymbol{\dot{X}}=[\dot{x}\ \dot{y}\ \dot{\alpha}]^T$ are the manipulator's velocities and $\boldsymbol{\dot{\Theta}}=[\dot{\theta_1}\ \dot{\theta_2}\ \dot{\theta_3}\ \dot{\delta_1}\ \dot{\delta_2}\ \dot{\delta_3}\ ]^T$ are the active joints' velocities. Matrix $\boldsymbol{A}$ is given by:

$$\boldsymbol{A}=\begin{bmatrix} a_{11} & a_{12} & a_{13} \\ a_{21} & a_{22} & a_{23} \\ a_{31} & a_{32} & a_{33} \end{bmatrix} \tag{8}$$

where $a_{n1}=l_2\cos\left(\beta_n\right)$, $a_{n2}=l_2\sin\left(\beta_n\right)$ and $a_{n3}=-l_2h\sin\left(\beta_n-\eta_n-\alpha\right)$, $n=1\ldots3$. And matrix $\boldsymbol{B}$ is given by:

$$\boldsymbol{B}=\begin{bmatrix} b_{11} & 0 & 0 & b_{14} & 0 & 0 \\ 0 & b_{22} & 0 & 0 & b_{15} & 0 \\ 0 & 0 & b_{33} & 0 & 0 & b_{16} \end{bmatrix} \tag{9}$$

where $b_{kk}=l_1l_2\sin\left(\beta_k-\theta_k\right)$ e $b_{k(k+3)}=l_2\cos\left(\beta_k-\gamma_k\right)$, where $k=1\ldots3$. The Jacobian matrix can be expressed as:

$$\boldsymbol{J}=\boldsymbol{A}^{-1}\boldsymbol{B} \tag{10}$$

3. SINGULARITY ANALYSIS

In Gosselin and Angeles (1990), three types of singularities for closed kinematic chains were defined based on the inverse and direct kinematic Jacobian matrices, i.e., respectively the matrices $\boldsymbol{A}$ and $\boldsymbol{B}$ shown in Eq. 7.

The first type occurs when $|\boldsymbol{A}|=0$, it is known as force uncertain or force unrestricted pose, here it will be called as direct singularity. The second type occurs when $|\boldsymbol{B}|=0$, it will be called here as inverse singularity. The last type occurs when both determinants are zero, $|\boldsymbol{A}|=|\boldsymbol{B}|=0$, and it is called combined singularity.

Singularity analysis for 3PRRR manipulators has already been done in other works, such as in Ebrahimi *et al.* (2007) and Ebrahimi *et al.* (2008a). The latter includes the analysis of other 3PRRR's configurations.

3.1 Local Conditioning Number(LCI)

LCI is based on the condition number of the manipulator's Jacobian matrix, which is defined as the ratio between the maximum and minimum singular values of the Jacobian matrix (Patel and Sobh, 2014), as shown in Eq. 11.

$$\kappa=\frac{\sigma_{max}}{\sigma_{min}} \tag{11}$$

where σ_{max} and σ_{min} are the maximum and minimum singular values of the Jacobian matrix, respectively. When the condition number approaches unity, it indicates that the manipulator approaches an isotropic configuration, i.e., a configuration with performance, regarding rigidity and precision, equal in all directions, with a precision close to its actuators (Ebrahimi *et al.*, 2008b). On the other hand, if the Jacobian matrix doesn't have full rank, this implies that the minimum singular value is zero, $\sigma_{min}=0$, and that the condition number tends to infinity. This occurs when the manipulator's configuration is singular. In this type of configuration, the performance is extremely poor in some directions, while in others, the performance is extremely good (Legnani *et al.*, 2010).

In order to avoid computation problems when the condition number tends to infinity, its reciprocal is used, Eq. 12, and is known as Local Conditioning Index (LCI).

$$\mathcal{K}=\frac{1}{\kappa} \tag{12}$$

The fact that the 3PRRR manipulator has two types of active joints implies that the Jacobian matrix is not dimensionally homogeneous. For the condition number and LCI to provide meaningful results, it is necessary to homogenize the Jacobian matrix (Alba-Gomez *et al.*, 2005). To achieve this, the elements of the third column of matrix $\boldsymbol{A}$, Eq. 8, were divided by a characteristic length, which was defined as $L_c = \sqrt{2}h$, as recommended in Alba-Gomez *et al.* (2005). In addition, the elements $b_{k(k+3)}$, with $k = 1, \ldots, 3$, of matrix $\boldsymbol{B}$ were multiplied by $\frac{p}{2\pi}$, where p is the prismatic joint's pitch.

3.2 NORMALISED SCALED INCIRCLE RADIUS (NSIR)

NSIR was presented in Ebrahimi *et al.* (2008b) for a 3RPRR manipulator. This index is based on geometric characteristics of the manipulator and its inverse kinematic Jacobian matrix. In this section, the procedure used to calculate the NSIR for a PRRR manipulator is explained.

With the kinematic analysis results it is possible to calculate the positions of the points A_i, B_i and C_i using the following relations:

$$A_i = a \begin{bmatrix} \cos(\lambda_i) \\ \sin(\lambda_i) \end{bmatrix} + \delta_i \begin{bmatrix} \cos(\gamma_i) \\ \sin(\gamma_i) \end{bmatrix} \tag{13}$$

$$B_i = A_i + l_1 \begin{bmatrix} \cos(\theta_i) \\ \sin(\theta_i) \end{bmatrix} \tag{14}$$

$$C_i = B_i + l_2 \begin{bmatrix} \cos(\beta_i) \\ \sin(\beta_i) \end{bmatrix} \tag{15}$$

Thereafter the angular coefficients m_i and linear coefficients n_i of the lines $\overrightarrow{B_iC_i}$ are calculated with Eq. 16 and Eq. 17, respectively.

$$m_i = \frac{y_{C_i} - y_{B_i}}{x_{C_i} - x_{B_i}} \tag{16}$$

$$n_i = y_{B_i} - m_i x_{B_i} \tag{17}$$

where x_{C_i} and y_{C_i} are the coordinates of the point C_i in relation to the base coordinate system. Similarly, x_{B_i} and y_{B_i} are point B's coordinates in relation to the base coordinate system.

The next step is to calculate the coordinates x_{T_i} and y_{T_i} of the vertices T_i created by the intersections between the lines $\overrightarrow{B_iC_i}$, they are shown in Fig. 3. Specifically T_1 is created by the intersection of the lines $\overrightarrow{B_1C_1}$ and $\overrightarrow{B_2C_2}$, T_2 is created by the intersection of $\overrightarrow{B_2C_2}$ and $\overrightarrow{B_3C_3}$, and T_3 is created by the intersection of $\overrightarrow{B_3C_3}$ and $\overrightarrow{B_1C_1}$. By equating the line equations, Eq. 17, that form each vertex and eliminating y_{T_i}, the coordinate x_{T_i} can be obtained. Then by Substituting x_{T_i} in Eq. 17, y_{T_i} can be obtained. Equation 18 and Equation 19 exemplify the process to obtain the coordinates x_{T_1} and y_{T_1} for the vetex T_1, respectively.

$$x_{T_1} = -\frac{n_2 - n_1}{m_2 - m_1} \tag{18}$$

$$y_{T_1} = m_1 x_{T_1} + n_1 \tag{19}$$

Then the lengths t_i of the distance between the vertices T_i are calculated. Specifically t_1 is the distance between T_1 and T_2, t_2 is the distance between T_2 and T_3, and t_3 is the distance between T_3 and T_1. These lengths are illustrated in Fig. 3. Equation 20 exemplifies the calculation of t_1.

$$t_1 = \sqrt{(x_{T_2} - x_{T_1})^2 + (y_{T_2} - y_{T_1})^2} \tag{20}$$

With the lengths t_i and the vertices T_i, the radius of the incircle created by the lines $\overrightarrow{B_iC_i}$ can be obtained with the following relation:

$$r = \frac{\begin{vmatrix} x_{T_1} & y_{T_1} & 1 \\ x_{T_2} & y_{T_2} & 1 \\ x_{T_3} & y_{T_3} & 1 \end{vmatrix}}{t_1 + t_2 + t_3} \tag{21}$$

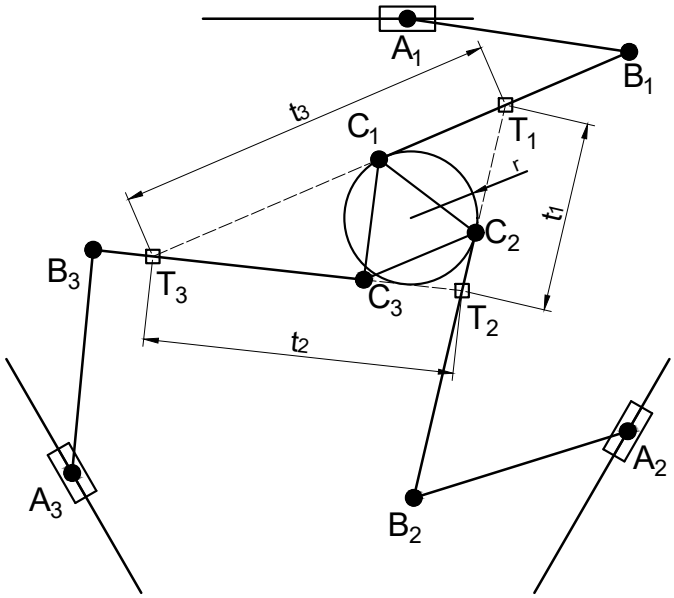

Figure 3: Representation of the inscribed circle used to calculate the NSIR.

Noting that the maximum radius coincides with the radius of the circle created by the vertices of the end-effector, i.e., $r_{max} = h$. Therefore, the radius calculated with Eq. 21 can be normalised dividing it by the r_{max}:

$$r_{norm} = \frac{r}{r_{max}} \tag{22}$$

The term r_{norm} is responsible for evaluating the closeness to direct singularities. The term responsible for evaluating the closeness to inverse singularities is derived from the inverse kinematic Jacobian matrix, $\boldsymbol{B}$, after its homogenization, as described in the last section.

$$\sqrt{|\boldsymbol{B}\boldsymbol{B}^T|} = \sqrt{\prod_{k=1}^{3}(b_{kk}^2 + b_{kk+3}^2)} = \sqrt{\prod_{k=1}^{3} l_1^2 l_2^2 \sin(\beta_k - \theta_k)^2 + \frac{l_2^2 p^2}{4\pi} cos(\beta_k - \gamma_k)^2} \tag{23}$$

When $\boldsymbol{B}\boldsymbol{B}^T = 0$ it signifies the occurrence of inverse singularities. Just like with r_{norm}, this term can also be normalised, noting that it has a superior limit of:

$$\sqrt{|\boldsymbol{B}\boldsymbol{B}^T|}_{max} = \sqrt{\left(l_1^2 l_2^2 + \frac{l_2^2 p^2}{4\pi}\right)^3} \tag{24}$$

Then the normalised term that represent the presence of inverse singularities is defined as:

$$\xi = \frac{\sqrt{|\boldsymbol{B}\boldsymbol{B}^T|}}{\sqrt{|\boldsymbol{B}\boldsymbol{B}^T|}_{max}} \tag{25}$$

Finally, the NSIR coefficient is obtained with the multiplication of both normalised terms:

$$\mathcal{N} = \xi r_{norm} \tag{26}$$

4. REDUNDANCY RESOLUTION SCHEMES

Optimization strategies used as redundancy resolution schemes can be classified into two categories: local and global. Global strategies search for the optimal solution considering the whole search space, while local strategies search for the optimal solution only within a region, or neighbourhood, of the search space. A global approach was used in this work.

It was composed of two optimization algorithms, the Genetic Algorithm (GA) and Sequential Quadratic Programming (SQP). First, the GA is applied, and its result is used as the starting point for the SQP.

The design variables of the redundancy resolution optimization problem were the redundant prismatic joints' positions, δ_i. Two approaches for this definition were used, both are more deeply explained in Fontes (2019). The first, and simpler, one was the prepositioning. In it the optimization procedure determines the best position for the redundant joints before the end-effector executes its trajectory. Therefore, the optimization problem in this case can be written as:

$$\begin{aligned} \max_{\delta_{i,fixed}} \quad & F(\delta_{i,fixed}) \\ \text{s.t.} \quad & \delta_{min} \leq \delta_{i,fixed} \leq \delta_{max} \end{aligned} \tag{27}$$

where $\delta_{i,fixed}$ are the positions of the redundant prismatic joints' that must be chosen and fixed before the task execution, δ_{min} and δ_{max} are respectively the minimum and maximum limits of the redundant joints, and $F(\delta_{i,fixed})$ is the objective function that is defined as one of the analyzed singularity avoidance indices, LCI and NSIR.

The second approach was called continuous positioning, in it the redundant joints move while the end-effector executes its trajectory. To achieve this it was defined a polynomial trajectory for the redundant joints. This polynomial was based on the initial and final positions, velocities and accelerations of the redundant joints, and it was a fifth order polynomial to allow the initial and final values for the accelerations to be assigned (Sciavicco and Siciliano, 2000). To ensure the smoothness of the polynomial, the initial and final velocities and accelerations were determined to be zero. So in this case, the design variables are the initial and final positions of the redundant prismatic joints. Therefore, the optimization problem in this case can be written as:

$$\begin{aligned} \max_{\delta_{o_i},\, \delta_{f_i}} \quad & F(\delta_{o_i},\, \delta_{f_i}) \\ \text{s.t.} \quad & \delta_{min} \leq \delta_{o_i} \leq \delta_{max} \\ & \delta_{min} \leq \delta_{f_i} \leq \delta_{max} \end{aligned} \tag{28}$$

where δ_{o_i} and δ_{f_i} are respectively the initial and final values for the redundant prismatic joints' positions that define the trajectory these joints will realize during the task's execution.

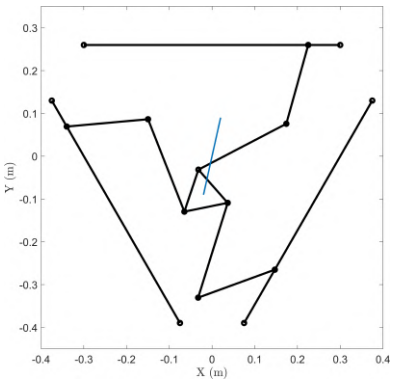

(a) Straight line

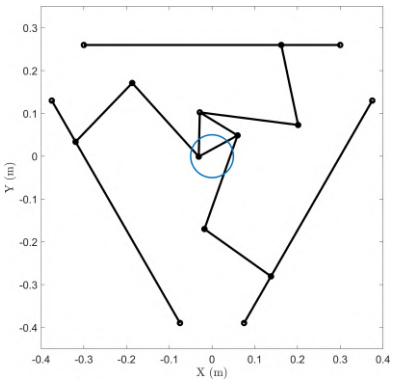

(b) Circle

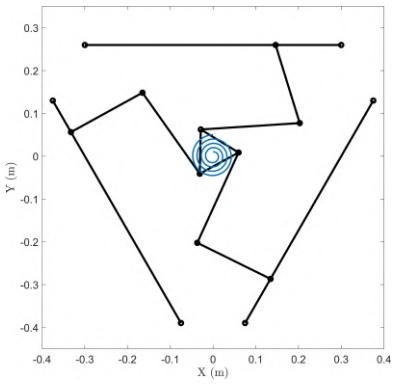

(c) Spiral

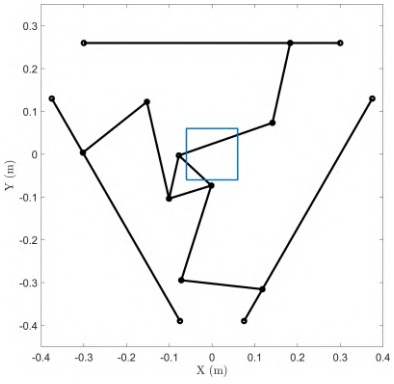

(d) Square

Figure 4: End-effector task trajectories.

Four tasks, or end-effector trajectories, were used. All of these trajectories are shown in Fig. 4. The first trajectory is a straight line beginning at the point $(x = -0.02\ m, y = -0,09\ m)$ with orientation $\alpha = 0.2\ rad$, and ending at the point $(x = 0.02\ m, y = 0.09\ m)$ with orientation $\alpha = 0\ rad$. The second trajectory is a circle with radius 0,05 m and center at the origin, it starts and ends at the point $(x = 0\ m, y = 0.05\ m)$ with orientation $\alpha = 0.5\ rad$. The third trajectory is an Archimedean spiral with $x = (0.01 + 0.0067\theta)\sin(2\pi\theta)$ and $y = (0.01 + 0.0067\theta)\cos(2\pi\theta)$, beginning at the point $(x = 0\ m, y = 0.01\ m)$ with orientation $\alpha = 0.5\ rad$, and ending at the point $(x = 0\ m, y = 0.05\ m)$ with orientation $\alpha = 0.5\ rad$. The last trajectory is a square with 0.12 m edge length, centered at the origin, it starts and ends at the point $(x = -0.06\ m, y = -0.06\ m)$ with orientation $\alpha = 0.3\ rad$.

5. RESULTS AND DISCUSSION

The results from the redundancy resolution simulations are summarized in Fig. 5 and Fig. 6 . Figure 5 shows the results with the prepositioning scheme, while Fig. 6 shows the results with the continuous positioning scheme.

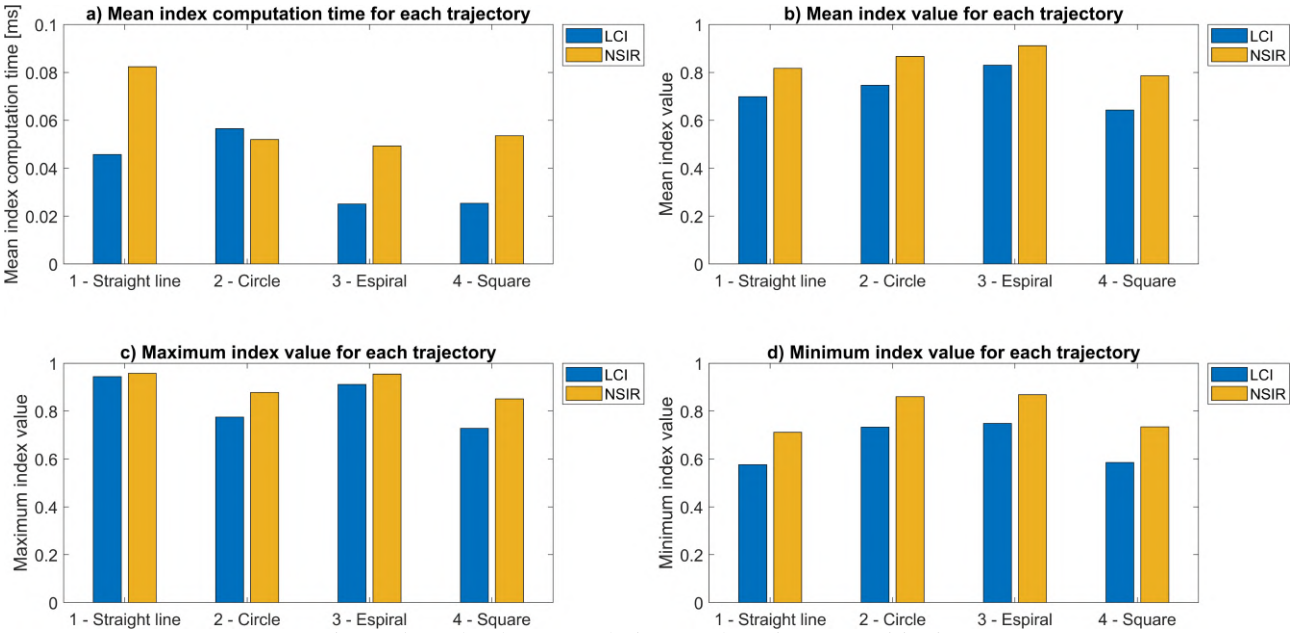

Figure 5: Redundancy resolution results using prepositioning.

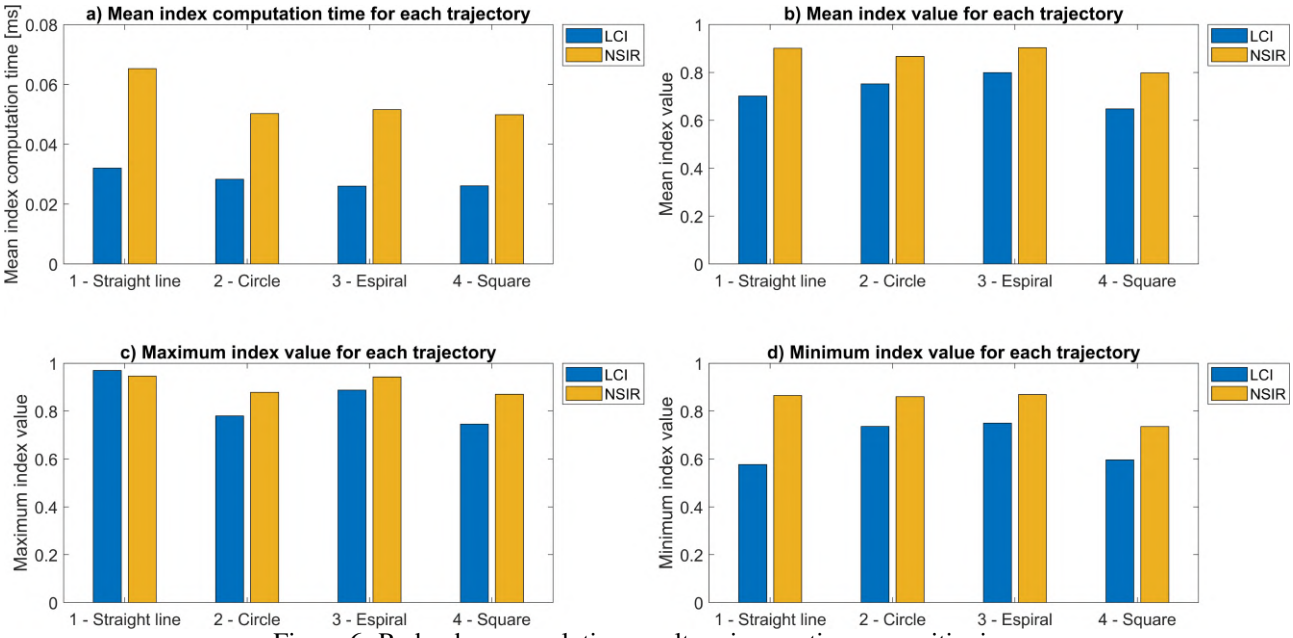

Figure 6: Redundancy resolution results using continuous positioning.

From the examination of the results, it can be noted that NSIR demands more processing time. This is indicated by the

fact that its mean computation time was longer than LCI's mean computation time for all cases, except in the combination prepositioning with circular end-effector trajectory, but even so by a small margin. This was expected due to the number of steps necessary to obtain the NSIR index.

Another point that can be inferred from the examination of the results is that the usage of NSIR seems to provide joint trajectories further away from singular configurations. This was indicated by the fact that in all cases the mean, maximum and minimum index values along the chosen joint trajectories were bigger when NSIR was used than when LCI was used, except for the maximum index value in the combination continuous positioning with straight line end-effector trajectory.

6. CONCLUSIONS

This paper compares two local singularity avoidance indices, LCI and NSIR, specifically for redundancy resolution optimization for planar parallel redundant manipulators. The results show that NSIR takes more time to be computed, but it provides better joint trajectories. Therefore it is recommended that NSIR is used for offline applications. In contrast, LCI should be used for online applications and other manipulators that fall outside the planar manipulators class in which the NSIR can be calculated. It would be interesting to add other indices, such as the Minimum Singular Value, or newly developed ones for future analyses.

ACKNOWLEDGMENTS

This research is supported by FAPESP 2018/21336-0. Felipe M. Farias Filho and Maíra M. da Silva are thankful for their scholarships CAPES 88887.511682/2020-00 and CNPq 301338/2018-3, respectively.

REFERENCES

Alba-Gomez, O., Wenger, P. and Pamanes, A., 2005. "Consistent Kinetostatic Indices for Planar 3-DOF Parallel Manipulators, Application to the Optimal Kinematic Inversion". In *Volume 7: 29th Mechanisms and Robotics Conference, Parts A and B*. ASMEDC, pp. 765–774. ISBN 0-7918-4744-6. doi:10.1115/DETC2005-84326. URL https://asmedigitalcollection.asme.org/IDETC-CIE/proceedings/IDETC-CIE2005/47446/765/314908.

Ebrahimi, I., Carretero, J.A. and Boudreau, R., 2007. "3-PRRR redundant planar parallel manipulator: Inverse displacement, workspace and singularity analyses". *Mechanism and Machine Theory*, Vol. 42, No. 8, pp. 1007–1016. ISSN 0094114X. doi:10.1016/j.mechmachtheory.2006.07.006. URL https://linkinghub.elsevier.com/retrieve/pii/S0094114X0600156X.

Ebrahimi, I., Carretero, J.A. and Boudreau, R., 2008a. "A family of kinematically redundant planar parallel manipulators". *Journal of Mechanical Design, Transactions of the ASME*, Vol. 130, No. 6, pp. 0623061–0623068. ISSN 10500472. doi:10.1115/1.2900723.

Ebrahimi, I., Carretero, J.A. and Boudreau, R., 2008b. "Kinematic analysis and path planning of a new kinematically redundant planar parallel manipulator". *Robotica*, Vol. 26, No. 3, pp. 405–413. ISSN 0263-5747. doi:10.1017/S0263574708004256.

Fontes, J.V.d.C., 2019. *Control of a Parallel Planar Manipulator with Kinematic Redundancy*. Thesis, Universidade de São Paulo, São Carlos. doi:10.11606/T.18.2019.tde-22052019-152125. URL http://www.teses.usp.br/teses/disponiveis/18/18162/tde-22052019-152125/.

Fontes, J.V.d.C. and Da Silva, M.M., 2016. "On the dynamic performance of parallel kinematic manipulators with actuation and kinematic redundancies". *Mechanism and Machine Theory*, Vol. 103, pp. 148–166. ISSN 0094114X. doi:10.1016/j.mechmachtheory.2016.05.004.

Gosselin, C.M. and Angeles, J., 1990. "Singularity Analysis of Closed-Loop Kinematic Chains". *IEEE Transactions on Robotics and Automation*, Vol. 6, No. 3, pp. 281–290. ISSN 1042296X. doi:10.1109/70.56660.

Gosselin, C.M. and Schreiber, L.T., 2018. "Redundancy in Parallel Mechanisms: A Review". *Applied Mechanics Reviews*, Vol. 70, No. 1. ISSN 0003-6900. doi:10.1115/1.4038931. URL https://asmedigitalcollection.asme.org/appliedmechanicsreviews/article/doi/10.1115/1.4038931/443694/Redundancy-in-Parallel-Mechanisms-A-Review.

Legnani, G., Tosi, D., Fassi, I., Giberti, H. and Cinquemani, S., 2010. "The "point of isotropy" and other properties of serial and parallel manipulators". *Mechanism and Machine Theory*, Vol. 45, No. 10, pp. 1407–1423. ISSN 0094114X. doi:10.1016/j.mechmachtheory.2010.05.007. URL https://linkinghub.elsevier.com/retrieve/pii/S0094114X10000844.

Merlet, J.P., 2006. *Parallel Robots*, Vol. 128 of *Solid Mechanics and Its Applications*. Springer-Verlag, Berlin/Heidelberg. ISBN 1-4020-4132-2. doi:10.1007/1-4020-4133-0. URL http://link.springer.com/10.1007/1-4020-4133-0.

Patel, S. and Sobh, T., 2014. "Manipulator Performance Measures - A Comprehensive Literature Survey". *Journal of Intelligent and Robotic Systems: Theory and Applications*, Vol. 77, No. 3-4, pp. 547–570. ISSN 15730409. doi:

10.1007/s10846-014-0024-y. URL https://link.springer.com/article/10.1007/s10846-014-0024-y.

Sciavicco, L. and Siciliano, B., 2000. *Modelling and Control of Robot Manipulators*. Advanced Textbooks in Control and Signal Processing. Springer London, London. ISBN 978-1-85233-221-1. doi:10.1007/978-1-4471-0449-0. URL http://link.springer.com/10.1007/978-1-4471-0449-0.

Wu, C., Liu, X.J., Xie, F. and Wang, J., 2011. "New measure for 'closeness' to singularities of parallel robots". In *Proceedings - IEEE International Conference on Robotics and Automation*. pp. 5135–5140. ISBN 9781612843865. ISSN 10504729. doi:10.1109/ICRA.2011.5979694.

Xie, F., Liu, X.J. and Li, J., 2014. "Performance indices for parallel robots considering motion/force transmissibility". *Lecture Notes in Computer Science (including subseries Lecture Notes in Artificial Intelligence and Lecture Notes in Bioinformatics)*, Vol. 8917, pp. 35–43. ISSN 16113349.

Yao, H., Li, Q., Chen, Q. and Chai, X., 2018. "Measuring the closeness to singularities of a planar parallel manipulator using geometric algebra". *Applied Mathematical Modelling*, Vol. 57, pp. 192–205. ISSN 0307904X. doi:10.1016/j.apm.2018.01.006. URL https://linkinghub.elsevier.com/retrieve/pii/S0307904X18300180.

RESPONSIBILITY NOTICE

The authors are solely responsible for the printed material included in this paper.